Characteristic Brain Distribution of 1-^{14}C-Octanoate in a Rat Model of Focal Cerebral Ischemia in Comparison with Those of ^{123}I-IMP and ^{123}I-Iomazenil

Yuji Kuge, PhD[1]; Kenji Hikosaka, MS[1,2]; Koh-ichi Seki, PhD[2]; Kazue Ohkura, PhD[2]; Ken-ichi Nishijima, MS[1,2]; Tomohito Kaji, BM[1]; Satoshi Ueno, BS[1]; Eriko Tsukamoto, MD[1]; and Nagara Tamaki, MD[1]

[1]Departments of Tracer Kinetics and Nuclear Medicine, Graduate School of Medicine, Hokkaido University, Sapporo, Japan; and [2]Faculty of Pharmaceutical Sciences, Health Science University of Hokkaido, Ishikari, Japan

1-^{11}C-Octanoate is a potential tracer for studying astroglial function in PET. To evaluate the usefulness of 1-^{11}C-octanoate for studying ischemic stroke, we investigated the brain distribution of 1-^{14}C-octanoate and compared it with *N*-isopropyl-*p*-^{123}I-iodoamphetamine (^{123}I-IMP) distribution (cerebral blood flow), ^{123}I-iomazenil (^{123}I-IMZ) distribution (neuronal viability based on ^{123}I-IMZ binding to benzodiazepine receptors), and hematoxylin–eosin stain (morphologic changes) in a rat model of focal cerebral ischemia. **Methods:** The right middle cerebral artery of each rat was occluded intraluminally. The brain distribution of 1-^{14}C-octanoate and ^{123}I-IMP (or ^{123}I-IMZ) was determined 4 and 24 h after the insult using a dual-tracer autoradiographic technique (n = 4–7 in each group). Coronal brain sections adjacent to those used for autoradiography were stained with hematoxylin and eosin. Regions of interest (ROIs) were determined for 3 coronal slices, and asymmetry indices (AIs, lesion/normal hemisphere) of the tracer uptake were calculated. ROIs on the hemisphere with the lesion were classified into 4 groups: In region A, widespread necrotic cells were observed; in region B, necrotic cells were occasionally observed; in region C1, no morphologic changes were observed and the AIs for ^{123}I-IMP (or ^{123}I-IMZ) were $\leq$0.8; and in region C2, no morphologic changes were observed and the AIs for ^{123}I-IMP (or ^{123}I-IMZ) were $>$0.8. **Results:** 1-^{14}C-Octanoate uptake decreased in the regions where morphologic changes were observed (regions A and B) but was relatively preserved in the surrounding region without morphologic changes despite reduced ^{123}I-IMP and ^{123}I-IMZ uptake (region C1). In the region without morphologic changes (region C1), AIs for 1-^{14}C-octanoate were significantly higher than those for ^{123}I-IMP (4 h, 0.73 $\pm$ 0.23 for 1-^{14}C-octanoate and 0.37 $\pm$ 0.20 for ^{123}I-IMP, $P <$ 0.0001; 24 h, 0.84 $\pm$ 0.11 for 1-^{14}C-octanoate and 0.44 $\pm$ 0.15 for ^{123}I-IMP, $P < 0.0001$) and those for ^{123}I-IMZ (4 h, 0.83 $\pm$ 0.19 for 1-^{14}C-octanoate and 0.57 $\pm$ 0.13 for ^{123}I-IMZ, $P < 0.0001$; 24 h, 0.91 $\pm$ 0.13 for 1-^{14}C-octanoate and 0.73 $\pm$ 0.06 for ^{123}I-IMZ, $P <$ 0.0001). **Conclusion:** 1-^{14}C-Octanoate uptake was relatively preserved in the regions without morphologic changes despite reduced ^{123}I-IMP and ^{123}I-IMZ uptake. 1-^{11}C-Octanoate may provide further functional information on the pathophysiology of ischemic stroke, reflecting astroglial function based on fatty acid metabolism.

Key Words: 1-^{11}C-octanoate; cerebral ischemia; glial function; neuronal function; cerebral blood flow

J Nucl Med 2003; 44:1168–1175

Although ischemic stroke is one of the most common neuronal disorders, the routine use of PET for the clinical assessment of pathophysiologic changes in the disease has been limited exclusively to the determination of cerebral blood flow (CBF) and oxygen and glucose metabolism (*1*), except for several laboratories. This restriction is due primarily to the lack of radiopharmaceuticals suitable for imaging the pathophysiology of ischemic stroke in clinical diagnosis of the disease. Recently, increasing interest has been focused on interactions between glial cells (particularly astrocytes) and neurons (*2–5*). It is now a matter of great importance to elucidate astroglial function, including metabolic function, in the pathophysiology of cerebral ischemia (*6,7*). The use of radiopharmaceuticals, combined with PET, for studying such astroglial function should provide useful information on the pathophysiology of the disease. To the best of our knowledge, however, there have been no reports concerning radiopharmaceuticals for imaging astroglial function, except for a preliminary report of Muir et al. (*8*). They proposed positron-labeled acetate and fluoroacetate as markers of glial cells, based on their basic studies with tritium-labeled compounds. However, the application of these compounds as in vivo imaging agents may be hampered by their low permeability of the blood–brain barrier (*9*).

Octanoate, an 8-carbon monocarboxylate, is converted to glutamine in astrocytes through the tricarboxylic acid cycle

Received Nov. 4, 2002; revision accepted Mar. 5, 2003.

For correspondence or reprints contact: Yuji Kuge, PhD, Department of Tracer Kinetics, Graduate School of Medicine, Hokkaido University, Kita 15 Nishi 7, Kita-ku, Sapporo 060-8638, Japan.

E-mail: kuge@med.hokudai.ac.jp

after β-oxidation (*10–15*), a process similar to the metabolism of acetate (*8,16*). In addition, octanoate is taken up in the brain more readily than are other mono-, di-, or tricarboxylic saturated fatty acids (*9,17,18*). Thus, a positron-labeled octanoate may be applicable as a PET tracer for studying cerebral astroglial function based on fatty acid metabolism and may be superior to positron-labeled acetate and fluoroacetate. In this regard, we previously evaluated the pharmacokinetic properties of radiolabeled octanoate and its derivatives in vitro (*19,20*) and in vivo (*15,21–23*) and demonstrated the potential of 1-^{11}C-octanoate as a PET tracer for studying such astroglial function. We also preliminarily assessed brain uptake of 1-^{11}C-octanoate in rat and canine models of focal cerebral ischemia (*24,25*).

In the present study, we investigated the brain distribution of 1-^{14}C-octanoate and compared it with *N*-isopropyl-*p*-^{123}I-iodoamphetamine (^{123}I-IMP) distribution (CBF), ^{123}I-iomazenil (^{123}I-IMZ) distribution (neuronal viability based on ^{123}I-IMZ binding to benzodiazepine receptors), and the results of hematoxylin–eosin (HE) staining (morphologic changes) in a rat model of focal cerebral ischemia, to further evaluate the usefulness of 1-^{11}C-octanoate for studying ischemic stroke.

MATERIALS AND METHODS

1-^{14}C-Octanoate in ethanol (radiochemical purity, >99%; specific activity, 1.96 GBq/mmol) was purchased from American Radiolabeled Chemicals Inc. The ethanol solution of 1-^{14}C-octanoate was evaporated under a nitrogen stream, and the residue was dissolved in physiologic saline (3.0 MBq/mL). ^{123}I-IMP and ^{123}I-IMZ were synthesized according to the methods reported previously (*26,27*). All other reagents used were of analytic grade.

Animal Preparation

The experimental protocol was fully approved by the Laboratory Animal Care and Use Committee of Hokkaido University. Male Sprague–Dawley rats weighing 300–350 g were used. The rats were allowed free access to water and laboratory chow.

The rats were anesthetized intraperitoneally using chloral hydrate (400 mg/kg body weight). The ostium of the right middle cerebral artery (MCA) in each rat was occluded intraluminally following a method described in detail previously (*28–30*). The rats were allowed to recover from anesthesia, and any induced neurologic deficits were confirmed. Rats not showing any neurologic deficits were excluded from the study.

Autoradiographic Studies

The brain distribution of 1-^{14}C-octanoate was determined and compared with CBF at 4 ($n = 4$) and 24 ($n = 4$) h after the insult using a dual-tracer autoradiographic technique with 1-^{14}C-octanoate and ^{123}I-IMP. A dose of 1-^{14}C-octanoate (3.0 MBq/kg body weight) was injected first through the femoral vein. ^{123}I-IMP (111 MBq/kg body weight) was then injected 5 min later through the contralateral femoral vein. These tracers were injected while the rats were under light ether anesthesia. Under ether anesthesia, the rats were sacrificed by decapitation 10 min after injection of 1-^{14}C-octanoate, which occurred 4 and 24 h after the insult. The brain distribution of 1-^{14}C-octanoate was also compared with ^{123}I-IMZ distribution, a marker of neuronal viability based on benzodiazepine receptor function, 4 ($n = 6$) and 24 ($n = 7$) h after the insult. A dose of ^{123}I-IMZ (111 MBq/kg body weight) was injected first through the femoral vein. Then, 50 min later, 1-^{14}C-octanoate (1.5 MBq/kg body weight) was injected through the contralateral femoral vein. These tracers were injected while the rats were under light ether anesthesia. Under ether anesthesia, the rats were sacrificed by decapitation 10 min after injection of 1-^{14}C-octanoate, which occurred 4 and 24 h after the insult.

The brains of the rats were removed and immersed in ice-cold saline. The brains were then sectioned at 2-mm thickness using a brain matrix (RBM-4000C; ASI Instruments) to obtain 8 coronal slices. The brain slices 4–6, 8–10, and 12–14 mm caudal from the frontal pole were incubated in a 1% solution of 2,3,5-triphenyltetrazolium chloride (TTC) at 37°C for vital staining. The brain slices 2–4, 6–8, and 10–12 mm caudal from the frontal pole were embedded in a medium (Tissue-Tek; Sakura Finetechnical Co., Ltd.), frozen in isopentane-dry ice, and cut into 20-μm sections with a cryostat (Bright Instrument Co., Ltd.).

The first autoradiographic exposure was performed for 3 h to detect the distribution of ^{123}I-IMP or ^{123}I-IMZ. The second exposure was initiated 10 d (18 half-lives of ^{123}I) later and performed for 3 d to image the distribution of 1-^{14}C-octanoate. It was preliminarily confirmed that the cross-contamination of ^{123}I and ^{14}C was less than 2%.

The coronal brain sections (20 μm) adjacent to those used for the autoradiographic studies were stained with HE.

Data Analysis

The autoradiographic images were analyzed using a computerized imaging analysis system (Bio-Imaging Analyzer BAS 5000; Fuji Photo Film). To quantitatively evaluate the distribution of 1-^{14}C-octanoate and ^{123}I-IMP, circular regions of interest (ROIs, 1.1 mm in diameter) were determined for 3 coronal brain slices as shown in Figure 1A. Because benzodiazepine receptor binding can reliably be assessed only in the cortex (*31*), only cortical regions were used for the comparative analysis of 1-^{14}C-octanoate and ^{123}I-IMZ. Asymmetry indices (AIs), defined as the ratios of values for an ROI in the right hemisphere to values for the contralateral homologous ROI and calculated after background subtraction, were used to exclude the effects associated with variations in levels of anesthesia. ROIs determined on the hemisphere with the lesion were classified visually in a masked manner into 3 groups based on the histologic findings of HE staining as follows (Table 1; Figs. 1B and 1C): In region A, widespread necrotic cells were observed; in region B, necrotic cells were occasionally observed; and in region C, no morphologic changes were observed. Cellular alterations such as pyknosis, eosinophilia, loss of hematoxylinophilia, scalloping, shrinkage, and swelling were considered necrotic, according to the criteria described by Garcia et al. (*32*). To characterize the 1-^{14}C-octanoate distribution in morphologically normal regions with reduced ^{123}I-IMP (or ^{123}I-IMZ) uptake, ROIs assigned for region C were further divided into 2 groups based on AIs for ^{123}I-IMP (or ^{123}I-IMZ): In region $C1_{IMP}$ (region $C1_{IMZ}$ for ^{123}I-IMZ), AIs for ^{123}I-IMP (or ^{123}I-IMZ) were ≤0.8; in region $C2_{IMP}$ (region $C2_{IMZ}$ for ^{123}I-IMZ), AIs for ^{123}I-IMP (or ^{123}I-IMZ) were >0.8 (Table 1). An AI threshold value, 0.8, was chosen, considering the lesion detectability of the autoradiographic methods (*33*).

The Bland–Altman plot (*34*), a graphical technique that helps assess agreement of 2 measurements, was used to compare AIs for

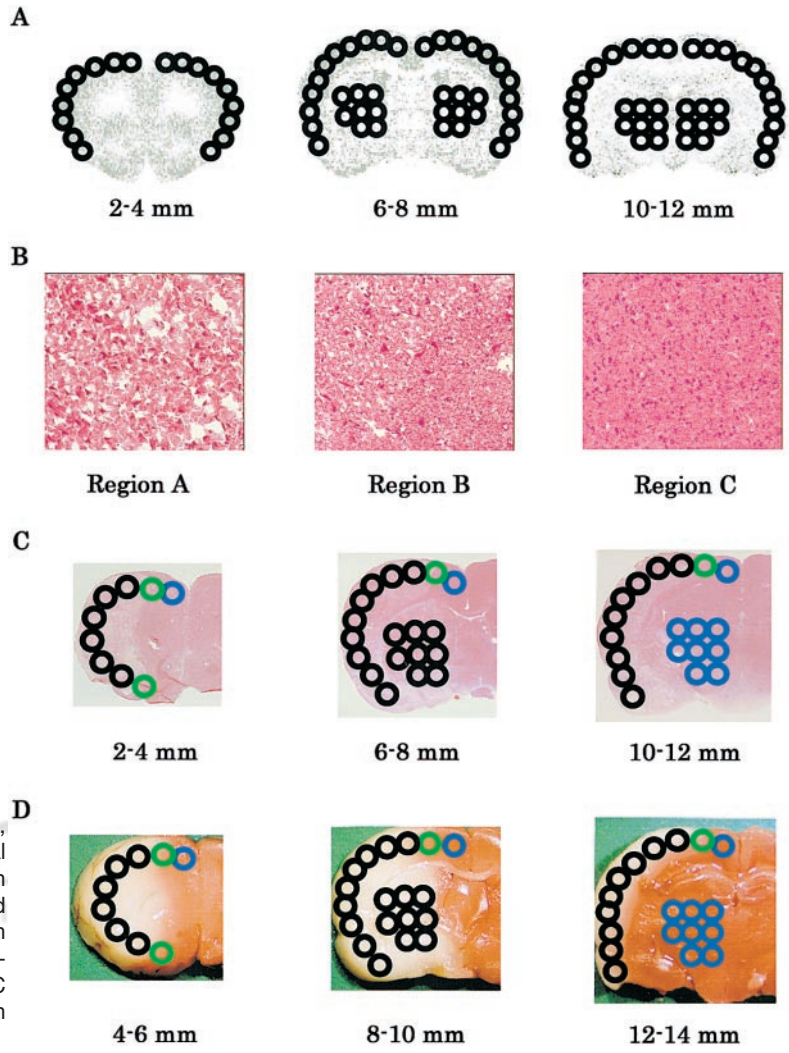

FIGURE 1. (A) Example of ROIs placed 2–4, 6–8, and 10–12 mm caudal from frontal pole on 3 coronal images. (B) Representative images of HE stain (×200). (C) Example of classified ROIs determined on images of HE stain. Black circle = region A; green circle = region B; blue circle = region C. (D) Approximate relationship of ROI classification with TTC stain. Black circle = region A; green circle = region B; blue circle = region C.

1-^{14}C-octanoate with those for ^{123}I-IMP or ^{123}I-IMZ. A paired *t* test was used to assess the significance of differences in AIs between ^{123}I-IMP (or ^{123}I-IMZ) and 1-^{14}C-octanoate. Statistical significance was determined using a 2-tailed value of $P < 0.05/4$ (i.e., 0.0125), considering a type I error rate for multiple comparisons.

RESULTS

Comparison with ^{123}I-IMP Distribution (CBF)

Figure 2 shows the representative images of TTC staining and autoradiograms for ^{123}I-IMP and 1-^{14}C-octanoate. Both ^{123}I-IMP uptake and 1-^{14}C-octanoate uptake were markedly decreased in the infarct regions (TTC-unstained region) at 4 and 24 h after the insult. In contrast, 1-^{14}C-octanoate uptake was relatively preserved in the periinfarct regions with reduced ^{123}I-IMP uptake.

Scattergrams and Bland–Altman plots (*34*) of AIs for ^{123}I-IMP versus AIs for 1-^{14}C-octanoate are shown in Figures 3A and 3B. In the regions where morphologic changes were observed (regions A and B), AIs for both ^{123}I-IMP and 1-^{14}C-octanoate markedly decreased at 4 and 24 h after the insult. In the region without morphologic changes (region C), particularly in region $C1_{IMP}$, 1-^{14}C-octanoate uptake was relatively preserved, compared with ^{123}I-IMP uptake.

Mean AIs for ^{123}I-IMP and 1-^{14}C-octanoate in each region are also summarized in Figures 3C and 3D. In region A, AIs were 0.09 ± 0.06 and 0.13 ± 0.24 for ^{123}I-IMP and 0.20 ± 0.15 and 0.14 ± 0.19 for 1-^{14}C-octanoate at 4 and 24 h, respectively, after the ischemic insult. The difference in AIs between ^{123}I-IMP and 1-^{14}C-octanoate was significant at 4 h ($P < 0.0001$). AIs in region B were 0.17 ± 0.08 and 0.54 ± 0.23 for ^{123}I-IMP and 0.29 ± 0.14 and 0.59 ± 0.28 for 1-^{14}C-octanoate at 4 and 24 h, respectively, after the insult.

TABLE 1
Classification of ROIs

Region	Histologic finding	AIs for ^{123}I-IMP or ^{123}I-IMZ
A	Widespread necrotic cells	—
B	Occasional necrotic cells	—
C1*	No morphologic changes	≤0.8
C2*	No morphologic changes	>0.8

*$C1_{IMP}$ and $C2_{IMP}$ for ^{123}I-IMP; $C1_{IMZ}$ and $C2_{IMZ}$ for ^{123}I-IMZ.

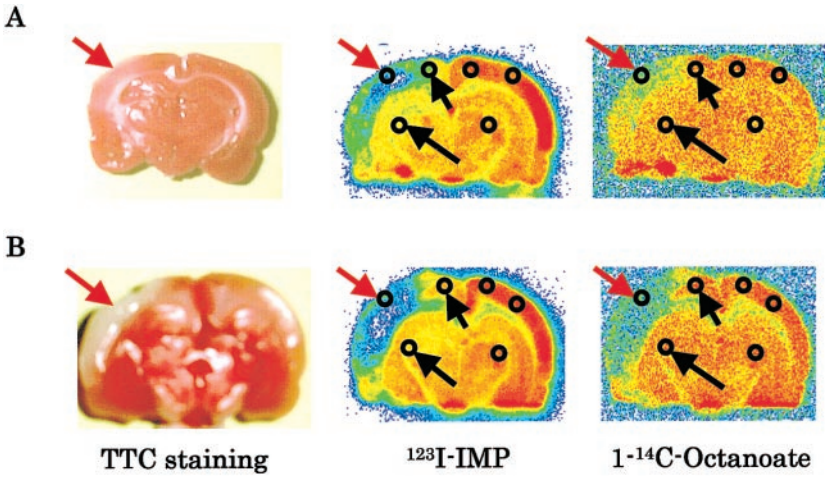

FIGURE 2. Representative images of TTC staining and autoradiograms for ^{123}I-IMP and 1-^{14}C-octanoate at 4 (A) and 24 (B) h after insult. 1-^{14}C-Octanoate uptake decreased in infarct regions (TTC-unstained region), indicated by red arrows, but was relatively preserved in periinfarct regions with reduced ^{123}I-IMP uptake, indicated by black arrows.

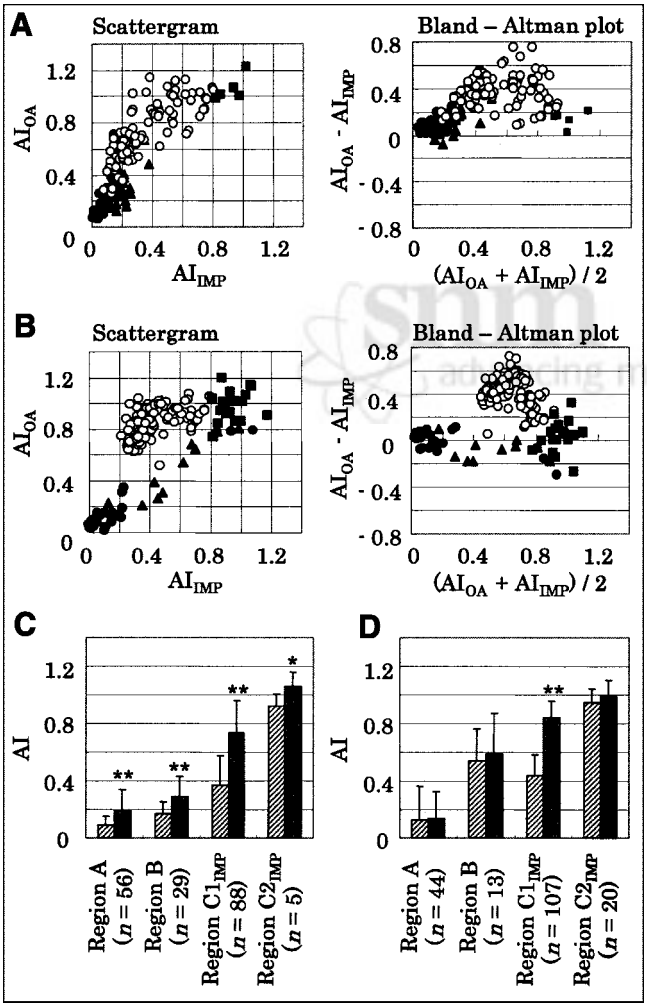

FIGURE 3. (A and B) Scattergrams and Bland–Altman plots between AIs for ^{123}I-IMP and AIs for 1-^{14}C-octanoate 4 (A) and 24 (B) h after insult. ● = region A; ▲ = region B; ○ = region $C1_{IMP}$; ■ = region $C2_{IMP}$, AI_{IMP} = AI for ^{123}I-IMP; AI_{OA} = AI for 1-^{14}C-octanoate; regions A, B, $C1_{IMP}$, and $C2_{IMP}$ are classified in Table 1. (C and D) AIs for ^{123}I-IMP and 1-^{14}C-octanoate in each region at 4 (C) and 24 (D) h after insult. Hatched bars = ^{123}I-IMP; solid bars = 1-^{14}C-octanoate. *$P < 0.0125$ vs. ^{123}I-IMP. **$P <$ 0.0001 vs. ^{123}I-IMP.

The difference in AIs between ^{123}I-IMP and 1-^{14}C-octanoate was significant at 4 h ($P < 0.0001$). In region $C1_{IMP}$, AIs for 1-^{14}C-octanoate were 0.73 ± 0.23 and 0.84 ± 0.11 at 4 and 24 h, respectively—significantly higher than those for ^{123}I-IMP (0.37 ± 0.20 at 4 h, $P < 0.0001$, and 0.44 ± 0.15 at 24 h, $P < 0.0001$). AIs in region $C2_{IMP}$ were 0.92 ± 0.09 and 0.95 ± 0.09 for ^{123}I-IMP and 1.06 ± 0.10 and 0.99 ± 0.12 for 1-^{14}C-octanoate at 4 and 24 h, respectively, after the insult. The difference in AIs between ^{123}I-IMP and 1-^{14}C-octanoate was significant at 4 h ($P < 0.0125$).

Comparison with ^{123}I-IMZ Distribution

The autoradiograms for ^{123}I-IMZ and 1-^{14}C-octanoate show that both ^{123}I-IMZ uptake and 1-^{14}C-octanoate uptake markedly decreased in the infarct regions (TTC-unstained region) at 4 and 24 h after the insult (Fig. 4). In contrast, 1-^{14}C-octanoate uptake was relatively preserved in the periinfarct regions with reduced ^{123}I-IMZ uptake.

AIs for 1-^{14}C-octanoate were markedly decreased at 4 and 24 h after the insult in the regions where morphologic changes were observed (regions A and B) (Figs. 5A and 5B). Relatively higher AIs for ^{123}I-IMZ were occasionally observed in these regions. In the region without morphologic changes (region C), particularly in region $C1_{IMZ}$, 1-^{14}C-octanoate uptake was relatively preserved, compared with ^{123}I-IMZ uptake.

In region A, AIs for 1-^{14}C-octanoate were 0.14 ± 0.11 and 0.24 ± 0.14 at 4 and 24 h, respectively, after the ischemic insult—significantly less than those for ^{123}I-IMZ (0.36 ± 0.23 at 4 h, $P < 0.0001$, and 0.43 ± 0.25 at 24 h, $P < 0.0001$) (Figs. 5C and 5D). AIs in region B were 0.52 ± 0.16 and 0.74 ± 0.17 for ^{123}I-IMZ and 0.50 ± 0.17 and 0.71 ± 0.16 for 1-^{14}C-octanoate at 4 and 24 h, respectively. The differences in AIs between ^{123}I-IMZ and 1-^{14}C-octanoate were not significant. In region $C1_{IMZ}$, AIs for 1-^{14}C-octanoate were 0.83 ± 0.19 and 0.91 ± 0.13 at 4 and 24 h, respectively—significantly higher than those for ^{123}I-IMZ (0.57 ± 0.13 at 4 h, $P < 0.0001$, and 0.73 ± 0.06 at 24 h, $P < 0.0001$). AIs in region $C2_{IMZ}$ were 0.87 ± 0.05 and 0.90 ± 0.09 for ^{123}I-IMZ and 1.05 ± 0.18 and 1.00 ±

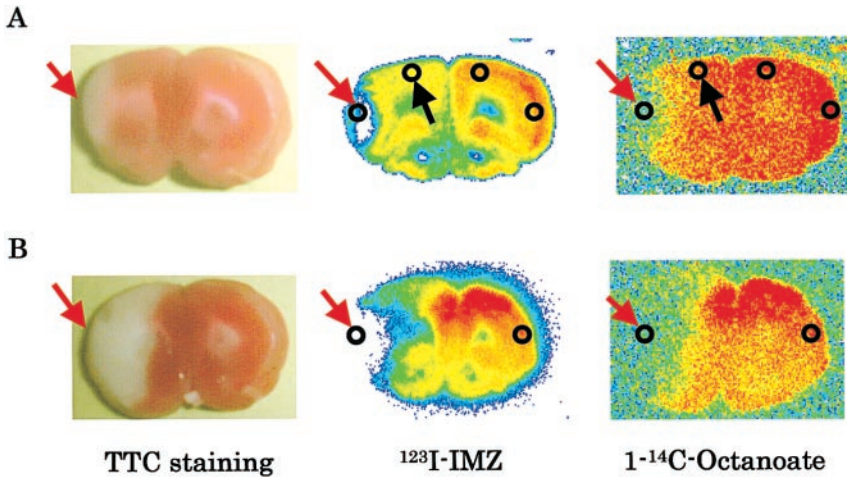

FIGURE 4. Representative images of TTC staining and autoradiograms for ^{123}I-IMZ and 1-^{14}C-octanoate at 4 (A) and 24 (B) h after insult. 1-^{14}C-Octanoate uptake decreased in infarct regions (TTC-unstained region), indicated by red arrows, but was relatively preserved in peri-infarct regions with reduced ^{123}I-IMZ uptake, indicated by black arrows.

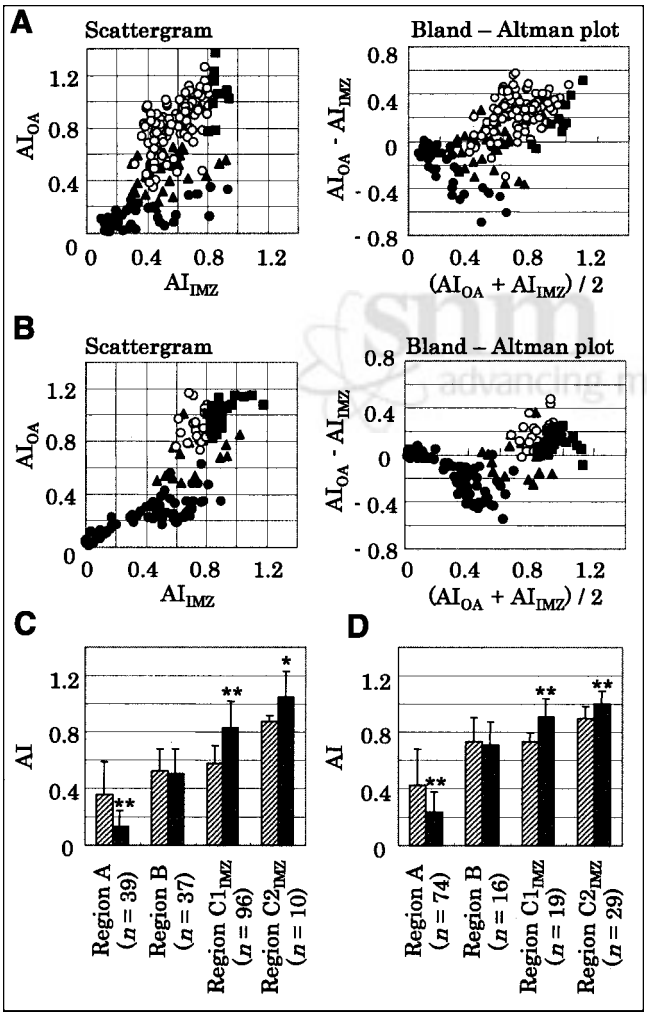

FIGURE 5. (A and B) Scattergrams and Bland–Altman plots between AIs for ^{123}I-IMZ and AIs for 1-^{14}C-octanoate at 4 (A) and 24 (B) h after insult. ● = region A; ▲ = region B; ○ = region $C1_{IMZ}$; ■ = region $C2_{IMZ}$, AI_{IMZ} = AI for ^{123}I-IMZ; AI_{OA} = AI for 1-^{14}C-octanoate; regions A, B, $C1_{IMZ}$, and $C2_{IMZ}$ are classified in Table 1. (C and D) AIs for ^{123}I-IMZ and 1-^{14}C-octanoate in each region at 4 (C) and 24 (D) h after insult. Hatched bars = ^{123}I-IMZ; solid bars = 1-^{14}C-octanoate. *$P < 0.0125$ vs. ^{123}I-IMZ. **$P <$ 0.0001 vs. ^{123}I-IMZ.

0.09 for 1-^{14}C-octanoate at 4 and 24 h, respectively, after the insult. These differences in AIs between ^{123}I-IMZ and 1-^{14}C-octanoate were also significant ($P < 0.0125$ for 4 h and $P < 0.0001$ for 24 h).

DISCUSSION

To evaluate the usefulness of 1-^{11}C-octanoate for studying ischemic stroke, we investigated the brain distribution of 1-^{14}C-octanoate and compared it with ^{123}I-IMP distribution (CBF), ^{123}I-IMZ distribution (neuronal viability based on ^{123}I-IMZ binding to benzodiazepine receptors), and the results of HE staining (morphologic changes) in a rat model of focal cerebral ischemia. 1-^{14}C-Octanoate uptake decreased in the regions where morphologic changes were observed (regions A and B) but was preserved in the region without morphologic changes despite reduced ^{123}I-IMP and ^{123}I-IMZ uptake (region C1). Thus, 1-^{14}C-octanoate showed the characteristic brain distribution in a rat model of focal cerebral ischemia, indicating that octanoate labeled with ^{11}C provides further functional information on the pathophysiology of ischemic stroke.

The present results show that an increased accumulation of 1-^{14}C-octanoate relative to CBF takes place in ischemic but viable regions, indicating that some mechanism responsible for the increased trapping of 1-^{11}C-octanoate–derived radioactivity is operating in these regions. These results are consistent with those of our previous study of a canine model of focal cerebral ischemia (*25*). Based on findings from previous studies on the brain uptake and metabolic aspects of octanoate (*13,15*), this trapping of radioactivity seems to be primarily attributable to 1-^{14}C-octanoate metabolites, most likely labeled glutamate and glutamine, in astrocytes. The important contribution of astrocytes to brain uptake of octanoate has also been demonstrated (*19,20*). The relatively preserved 1-^{14}C-octanoate uptake appears to reflect astroglial function based on octanoate metabolism.

^{123}I-IMZ, a benzodiazepine partial-inverse agonist, has been developed to permit SPECT investigation of central benzodiazepine receptors and used for the detection of

viable cortical neurons in ischemic stroke (*33*,*35*–*37*). Our results showed that uptake of 1-^{14}C-octanoate and ^{123}I-IMZ decreased in the region where necrotic cells were occasionally observed (region B), whereas AIs for 1-^{14}C-octanoate were significantly higher than those for ^{123}I-IMZ in the region without morphologic changes (region C). It is well known that glial cells are less sensitive to ischemic stress than are neurons (*38*–*40*). These findings also support the potential of radiolabeled octanoate for studying ischemic stroke as a marker of glial function.

The clinical use of PET for the assessment of pathophysiologic changes in ischemic stroke has been limited almost exclusively to the determination of CBF and of oxygen and glucose metabolism (*1*). 1-^{11}C-Octanoate may provide us with a unique means of elucidating the pathophysiology of ischemic stroke. Particularly, 1-^{11}C-octanoate, combined with ^{18}F-FDG, may be useful for achieving better understanding of the contributions of glial cells to brain function and interactions between neurons and glial cells and may provide further diagnostic values for patients with ischemic stroke. It remains unclear, however, whether preserved 1-^{14}C-octanoate uptake in the ischemic regions implies salvageable tissues or not. The precise mechanism underlying the trapping of octanoate, and the functions that are actually imaged by radiolabeled octanoate, also remain to be elucidated. Ischemic responses, such as astroglial activation, increased oxygen extraction rate, tissue acidosis, and changes in glutamate turnover, may influence the brain distribution of octanoate. Further studies, particularly those on the relationship between octanoate accumulation and the pathophysiology of cerebral ischemia, including oxygen and glucose metabolism and glial reactions, are required to clarify our understanding of this process.

1-^{11}C-Octanoate is readily synthesized in reproducible high yields using a Grignard reaction of ^{11}C-CO_2 with heptylmagnesium bromide and a commercially available automated synthetic apparatus. The availability of this procedure is expected to favor the clinical application of 1-^{11}C-octanoate. Conversely, clinical application of 1-^{11}C-octanoate may be restricted by the intricacy of its metabolism, which renders analysis of its pharmacokinetics difficult. Developing kinetic models for the analysis of the pharmacokinetics of 1-^{11}C-octanoate in the brain should ultimately prove to be of great benefit.

In the present study, the Bland–Altman plot (*34*) was used to assess the difference in AIs between 1-^{14}C-octanoate and ^{123}I-IMP (or ^{123}I-IMZ). This graphical technique clearly showed that the AIs for 1-^{14}C-octanoate were relatively higher than those for ^{123}I-IMP and ^{123}I-IMZ in the regions without morphologic changes (region C1), indicating that 1-^{14}C-octanoate uptake was relatively preserved in the region (region C1), compared with ^{123}I-IMP and ^{123}I-IMZ uptake.

It is important to consider several methodologic aspects in the present study. In a clinical setting, several hours are required to sufficiently characterize benzodiazepine receptor distribution after ^{123}I-IMZ injection. In this study, however, rats were sacrificed at 60 min after ^{123}I-IMZ administration, according to the method reported by Toyama et al. (*37*). They indicated by a kinetic study that specific binding of ^{123}I-IMZ can be evaluated at 60 min after injection in a rat model of cerebral ischemia. Specific distribution of ^{123}I-IMZ appears to be achieved within a shorter time of 60 min in rats. Ex vivo uptake (binding) studies using 1-^{14}C-octanoate and ^{123}I-IMZ are helpful to confirm this point and to further characterize 1-^{14}C-octanoate uptake in the brain. Such ex vivo studies, however, remain to be performed.

Although ^{123}I-IMZ, a benzodiazepine partial-inverse agonist, has been used as a marker of neuronal viability, ^{123}I-IMZ uptake decreased in the region $C1_{IMZ}$, where no necrotic neurons were observed. These results indicate that impairment of ^{123}I-IMZ accumulation, namely impairment of ^{123}I-IMZ binding to benzodiazepine receptors, precedes necrotic cellular alterations such as pyknosis, eosinophilia, loss of hematoxylinophilia, scalloping, shrinkage, and swelling. Structural and functional alterations of benzodiazepine receptors, including receptor regulation and transmitter competition, can be potential factors contributing to the altered ^{123}I-IMZ accumulation.

In the ischemic core (region A), accumulation of ^{123}I-IMZ was significantly higher than that of 1-^{14}C-octanoate (Figs. 5C and 5D). The higher accumulation of ^{123}I-IMZ may be ascribed to the destruction of the blood–brain barrier and the increased nonspecific binding of ^{123}I-IMZ, as the lipophilicity of ^{123}I-IMZ is higher than that of 1-^{14}C-octanoate. Another possible explanation for the results is the difference in the times of sacrifice after administration of ^{123}I-IMZ and 1-^{14}C-octanoate. A longer time after administration of the tracer may cause higher accumulation of the tracer in the ischemic core with severely reduced CBF. Matsuda et al. (*35*) and Toyama et al. (*37*) compared ^{123}I-IMZ distribution with CBF in rat models of cerebral ischemia and observed a relatively preserved ^{123}I-IMZ accumulation in the ischemic core.

Higher accumulations of ^{123}I-IMP, ^{123}I-IMZ, and 1-^{14}C-octanoate were observed in region B at 24 h than at 4 h. The reasons for the discrepancy remain unclear. The pathophysiology in the region at 24 h may be functionally different from that at 4 h, although necrotic cells were occasionally observed in these regions. The limited number of ROIs assigned to region B may be another reason for the discrepancy. The time points of sacrifice after the ischemic insult were also limited. Further studies, particularly detailed histologic evaluations using a larger number of animals at different time points, are required to clarify the reasons for the discrepancy.

CONCLUSION

The present study demonstrated that 1-^{14}C-octanoate uptake was relatively preserved in the regions without morphologic changes, compared with ^{123}I-IMP and ^{123}I-IMZ uptake. The relatively preserved 1-^{14}C-octanoate accumulation may reflect astroglial function based on fatty acid

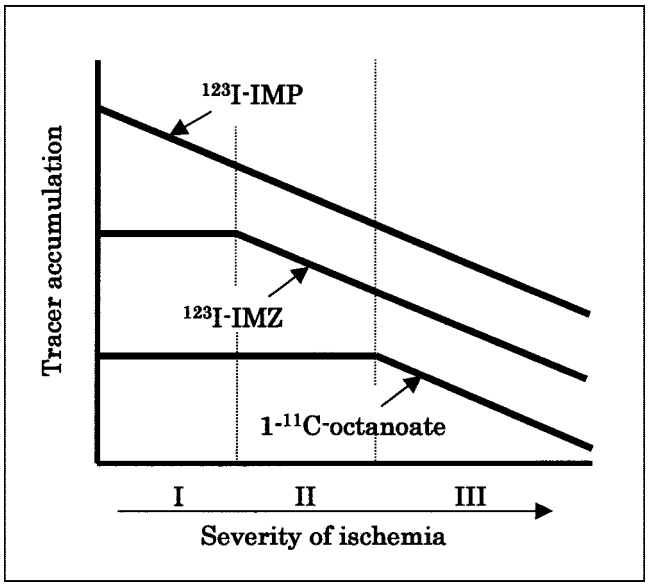

FIGURE 6. Schematic representation of possible relationship between tracer accumulation and cerebral function. I = preserved neuronal and astroglial function; II = impaired neuronal function and preserved astroglial function; III = impaired neuronal and astroglial function.

metabolism. Thus, a possible relationship between the tracer accumulation and the pathologic changes can be summarized as shown in Figure 6. Namely, ^{123}I-IMP accumulation decreases concurrently with CBF after the ischemic insult. ^{123}I-IMZ and 1-^{14}C-octanoate uptake is preserved at the stage with preserved neuronal and astroglial function. ^{123}I-IMZ uptake then decreases with impaired neuronal function based on benzodiazepine receptor binding. Finally, 1-^{14}C-octanoate uptake decreases with impaired astroglial function.

The present results provided a useful basis for the development of 1-^{11}C-octanoate as a PET tracer for studying the pathophysiology of ischemic stroke. 1-^{11}C-Octanoate warrants further evaluation as an in vivo indicator of astroglial function based on fatty acid metabolism.

ACKNOWLEDGMENTS

This work was supported in part by a grant from the Hokkaido Foundation for the Promotion of Scientific and Industrial Technology. The authors are grateful to Prof. Shinzo Nishi and Prof. Toshiyuki Ohnishi of the Central Institute of Isotope Science, Hokkaido University, for supporting this work.

REFERENCES

1. Heiss W-D, Herholz K. Assessment of pathophysiology of stroke by positron emission tomography. *Eur J Nucl Med.* 1994;21:455–465.
2. Tsacopoulos M, Magistretti PJ. Metabolic coupling between glia and neurons. *J Neurosci.* 1996;16:877–885.
3. Magistretti PJ, Pellerin L. Cellular bases of brain energy metabolism and their relevance to functional brain imaging: evidence for a prominent role of astrocytes. *Cereb Cortex.* 1996;6:50–61.
4. Magistretti PJ, Pellerin L. Astrocytes couple synaptic activity to glucose utilization in the brain. *News Physiol Sci.* 1999;14:177–182.
5. Araque A, Carmignoto G, Haydon PG. Dynamic signaling between astrocytes and neurons. *Annu Rev Physiol.* 2001;63:795–813.
6. Zoli M, Grimaldi R, Ferrari R, Zini I, Agnati LF. Short- and long-term changes in striatal neurons and astroglia after transient forebrain ischemia in rats. *Stroke.* 1997;28:1049–1059.
7. Louw DF, Masada T, Sutherland GR. Ischemic neuronal injury is ameliorated by astrocyte activation. *Can J Neurol Sci.* 1998;25:102–107.
8. Muir D, Berl S, Clarke DD. Acetate and fluoroacetate as possible markers for glial metabolism in vivo. *Brain Res.* 1986;380:336–340.
9. Oldendorf WH. Carrier-mediated blood-brain barrier transport of short-chain monocarboxylic organic acids. *Am J Physiol.* 1973;224:1450–1453.
10. Auestad N, Korsak RA, Morrow JW, Edmond J. Fatty acid oxidation and ketogenesis by astrocytes in primary culture. *J Neurochem.* 1991;56:1376–1386.
11. Edmond J, Robbins RA, Bergstrom JD, Cole RA, de Vellis J. Capacity for substrate utilization in oxidative metabolism by neurons, astrocytes and oligodendrocytes from developing brain in primary culture. *J Neurosci Res.* 1987;18:551–561.
12. Edmond J. Energy metabolism in developing brain cells. *Can J Physiol Pharmacol.* 1992;70:S118–S129.
13. Cremer JE, Teal HM, Heath DF, Cavanagh JB, The influence of portacaval anastomosis on the metabolism of labelled octanoate, butyrate and leucine in rat brain. *J Neurochem.* 1977;28:215–222.
14. Norenberg MD, Martinez-Hernandez A. Fine structural localization of glutamine synthetase in astrocytes of rat brain. *Brain Res.* 1979;161:303–310.
15. Kuge Y, Yajima K, Kawashima H, Yamazaki H, Hashimoto N, Miyake Y. Brain uptake and metabolism of [1-^{11}C]octanoate in rats: pharmacokinetic basis for its application as a radiopharmaceutical for studying brain fatty acid metabolism. *Ann Nucl Med.* 1995;9:137–142.
16. Berl S, Clarke DD. Compartmentation of amino acid metabolism. In: Lajtha A, ed. *Handbook of Neurochemistry*. Vol 2. New York, NY: Plenum; 1969:447–472.
17. Rowley H, Collins RC. [1-^{14}C]Octanoate: a fast functional marker of brain activity. *Brain Res.* 1985;335:326–329.
18. Spector R. Fatty acid transport through the blood-brain barrier. *J Neurochem.* 1988;50:639–643.
19. Yamazaki S, Fukui K, Kawashima H, Kuge Y, Miyake Y, Kangawa K. Uptake of radioactive octanoate in astrocytoma cells: basic studies for application of [^{11}C]octanoate as a PET tracer. *Ann Nucl Med.* 1996;10:395–399.
20. Kuge Y, Hikosaka K, Seki K, et al. *In vitro* uptake of [1-^{14}C]octanoate in brain slices of rats: basic studies for assessing [1-^{11}C]octanoate as a PET tracer of glial functions. *Nucl Med Biol.* 2002;29:303–306.
21. Kawashima H, Yajima K, Kuge Y, Hashimoto N, Miyake Y. Synthesis of [1-^{11}C]-2-octynoic acid, [1-^{11}C]-2-decynoic acid and [1-^{11}C]-3-(R, S)-methyl-octanoic acid as potential markers for PET studies of fatty acid metabolism. *J Labelled Compds Radiopharm.* 1997;39:181–193.
22. Kawashima H, Kuge Y, Yajima K, Miyake Y, Hashimoto N. Development of step-specific PET tracers for studying fatty acid β-oxidation: biodistribution of [1-^{11}C]octanoate analogs in rats and a cat. *Nucl Med Biol.* 1998;25:543–548.
23. Kuge Y, Kawashima H, Yamazaki S, Hashimoto N, Miyake Y. [1-^{11}C]Octanoate as a potential PET tracer for studying glial functions: PET evaluation in rats and cats. *Nucl Med Biol.* 1996;23:1009–1012.
24. Kuge Y, Kawashima H, Hashimoto N, et al. Preliminary evaluation of [1-^{11}C]octanoate as a PET tracer for studying cerebral ischemia. *Ann Nucl Med.* 2000;14:69–74.
25. Kuge Y, Kawashima H, Minematsu K, et al. [1-^{11}C]Octanoate as a PET tracer for studying ischemic stroke: evaluation in a canine model of thromboembolic stroke with positron emission tomography. *Biol Pharm Bull.* 2000;23:984–988.
26. Kuhl DE, Barrio JR, Huang SC, et al. Quantifying local cerebral blood flow by N-isopropyl-p-[^{123}I]iodoamphetamine (IMP) tomography. *J Nucl Med.* 1982;23:196–203.
27. McBrides BJ, Baldwin RM, Kerr JM, Wu JL. A simple method for the preparation of ^{123}I-and ^{125}I-labeled iodobenzodiazepines. *Appl Radiat Isot.* 1991;42:173–175.
28. Longa EZ, Weinstein PR, Carlson S, Cummins R. Reversible middle cerebral artery occlusion without craniectomy in rats. *Stroke.* 1989;20:84–91.
29. Minematsu K, Li L, Fisher M, Sotak CH, Davis MA, Fiandaca MS. Diffusion-weighted magnetic resonance imaging: rapid and quantitative detection of focal brain ischemia. *Neurology.* 1992;42:235–240.
30. Kuge Y, Minematsu K, Yamaguchi T, Miyake Y. Nylon monofilament for intraluminal middle cerebral artery occlusion in rats. *Stroke.* 1995;26:1655–1658.
31. Heiss W-D, Kracht L, Grond M, et al. Early [^{11}C]flumazenil/H_2O positron

emission tomography predicts irreversible ischemic cortical damage in stroke patients receiving acute thrombolytic therapy. *Stroke.* 2000;31:366–369.
32. Garcia JH, Liu KF, Ho KL. Neuronal necrosis after middle cerebral artery occlusion in Wistar rats progresses at different time intervals in the caudoputamen and the cortex. *Stroke.* 1995;26:636–642.
33. Watanabe Y, Nakano T, Yutani K, et al. Detection of viable cortical neurons using benzodiazepine receptor imaging after reversible focal ischaemia in rats: comparison with regional cerebral blood flow. *Eur J Nucl Med.* 2000;27:308–313.
34. Bland JM, Altman DG. Statistical methods for assessing agreement between two methods of clinical measurement. *Lancet.* 1986;327:307–310.
35. Matsuda H, Tsuji S, Kuji I, Shiba K, Hisada K, Mori H. Dual-tracer autoradiography using ^{125}I-iomazenil and 99Tcm-HMPAO in experimental brain ischaemia. *Nucl Med Commun.* 1995;16:581–590.
36. Hatazawa J, Satoh T, Shimosegawa E, et al. Evaluation of cerebral infarction with iodine 123-iomazenil SPECT. *J Nucl Med.* 1995;36:2154–2161.
37. Toyama H, Matsumura K, Nakashima H, et al. Characterization of neuronal damage by iomazenil binding and cerebral blood flow in an ischemic rat model. *Ann Nucl Med.* 1998;12:267–273.
38. Lassen NA. Incomplete cerebral infarction: focal incomplete ischemic tissue necrosis not leading to emollision. *Stroke.* 1982;13:522–523.
39. Marcoux FW, Morawetz RB, Crowell RM, DeGirolami U, Halsey JH Jr. Differential regional vulnerability in transient focal cerebral ischemia. *Stroke.* 1982; 13:339–346.
40. Garcia JH, Kamijyo Y. Cerebral infarction: evolution of histopathological changes after occlusion of a middle cerebral artery in primates. *J Neuropathol Exp Neurol.* 1974;33:408–421.

The Journal of NUCLEAR MEDICINE

Characteristic Brain Distribution of 1-^{14}C-Octanoate in a Rat Model of Focal Cerebral Ischemia in Comparison with Those of ^{123}I-IMP and ^{123}I-Iomazenil

Yuji Kuge, Kenji Hikosaka, Koh-ichi Seki, Kazue Ohkura, Ken-ichi Nishijima, Tomohito Kaji, Satoshi Ueno, Eriko Tsukamoto and Nagara Tamaki

J Nucl Med. 2003;44:1168-1175.

The Journal of Nuclear Medicine is published monthly.
SNMMI | Society of Nuclear Medicine and Molecular Imaging
1850 Samuel Morse Drive, Reston, VA 20190.
(Print ISSN: 0161-5505, Online ISSN: 2159-662X)

SNMMI SOCIETY OF NUCLEAR MEDICINE AND MOLECULAR IMAGING